TECHNISCHE UNIVERSITÄT DRESDEN

Fakultät Informatik

TECHNISCHE BERICHTE
TECHNICAL REPORTS

ISSN 1430-211X

TUD-FI19-03-August 2019

Somnath Dutta, Benjamin Russig, Stefan Gumhold

Chair of Computer Graphics & Visualization

Moving Least Squares Correspondences for Iterative Point Set Registration

TechnischeUniversität Dresden
Nutzerberatung CD
01062 Dresden
Germany
http://tu-dresden.de/cd

DRESDEN concept
Exzellenz aus Wissenschaft und Kultur

Moving Least Squares Correspondences for Iterative Point Set Registration

Somnath Dutta[1], Benjamin Russig[1] and Stefan Gumhold[1]
[1]*Chair of Computer Graphics & Visualization, TU Dresden, Germany*
{*somnath.dutta, benjamin.russig, stefan.gumhold*}*@tu-dresden.de*

Abstract

Registering partial shapes plays an important role in numerous applications in the fields of robotics, vision, and graphics. An essential problem of registration algorithms is the determination of correspondences between surfaces. In this paper, we provide a in-depth evaluation of an approach that computes high-quality correspondences for pair-wise closest point-based iterative registration and compare the results with state-of-the-art registration algorithms. Instead of using a discrete point set for correspondence search, the approach is based on a locally reconstructed continuous moving least squares surface to overcome sampling mismatches in the input shapes. Furthermore, MLS-based correspondences are highly robust to noise. We demonstrate that this strategy outperforms existing approaches in terms of registration accuracy by combining it with the SparseICP local registration algorithm. Our extensive evaluation over several thousand scans from different sources verify that MLS-based approach results in a significant increase in alignment accuracy, surpassing state-of-the-art feature-based and probabilistic methods. At the same time, it allows an efficient implementation that introduces only a modest computational overhead.

1 Introduction

The acquisition of 3D geometry from physical objects has increasingly gained popularity in the last decades. Many scanning techniques follow a sequential scanning paradigm where an object or scene is scanned several times from different view points. The result of this acquisition process is a set of scans, each given in a local coordinate system defined by the pose of the scanning device. To allow the reconstruction of a complete model, these scans have to be transformed into a common coordinate system, in which further processing is possible. The accuracy of this registration step is of significant importance to the quality of the final model as registration errors may lead to artificial creases and reconstruction artifacts like oscillations or even holes.

The goal of pairwise registration is to find a transform that aligns a source scan in a way that it is as close as possible to the surface represented by a target scan, ignoring the non-overlapping parts. This objective is formalized differently by several registration methods. Variants of the Iterative Closest Point method ICP (Besl and McKay, 1992) formulate a two-stage strategy: The first stage estimates correspondences between the two scans, and the second stage optimizes the transform so as to minimize the residual errors of the correspondences. Alternating between these two stages, ICP converges to a local optimizer.

The quality of the estimated correspondences has a significant impact on the performance of such ICP variants. Better correspondences (in the sense of being a more faithful representation of the underlying geometry) usually improve convergence and yield more accurate results. Many ICP variants still use direct correspondences between the two scans (represented as point clouds). Hence, a point of the source scan is usually in correspondence with one of the finitely many points of the target scan. This has two drawbacks to be addressed: (1) Noise and outliers in the point clouds transfer directly to the correspondences, which slows down convergence. (2) Two different scans do not in general sample the model surface at the same locations. This sampling discrepancy and the discrete matching limits the accuracy of the final registration result.

To overcome these drawbacks, (Huang Y et al., 2011) proposed moving least squares (MLS) correspondences, which are effective for ICP variants. The MLS correspondence scheme projects the points of the source scan onto the MLS surface represented by the target scan. Therefore, the corresponding target points are not restricted to sample locations, which makes the scheme insensitive to discrepancies in the sampling. Furthermore, the locally reconstructed MLS surface is in general closer to the actual underlying surface due to its de-noising properties. In prac-

tice, this feature improves the convergence behavior of iterative optimizers like ICP as shown in the evaluation section. We overcome the limited evaluation of the MLS Correspondences by (Huang Y et al., 2011) with a detailed analysis on state of the art datasets to validate the efficiency of the MLS correspondence approach. The method can be directly used in any iterative registration method without further modification. We showcase this property by augmenting the Sparse-ICP framework (Bouaziz et al., 2013) with the MLS correspondence determination. To minimize the effect of outliers in the determined correspondence, we introduce two different filtering strategy based on normal angle between the corresponding point and the other incorporates higher order geometric information, i.e. mean curvature for filtering correspondences as detailed in section 4.

Our evaluation confirms that MLS-based correspondences achieve a significantly higher level of registration accuracy than other correspondence computation approaches while adding only a modest computational overhead.

2 STATE OF THE ART

Registration is a widely researched problem with vast applicability in various domains like 3D scanning, shape analysis, or motion capturing. For an overview of existing registration algorithms, we refer the reader to the respective surveys (Rusinkiewicz and Levoy, 2001; Salvi et al., 2007; Tam et al., 2013; Bellekens et al., 2014). In the following, we will briefly outline the types of registration methods that can benefit from MLS correspondences.

According to the aforementioned surveys, registration approaches can be classified w.r.t. to the following criteria:

Pairwise / Multi-Way Pairwise registration methods aim at registering two partially overlapping scans. Overall registration of a data set can be achieved by successively adding scans and registering them to their predecessors or to all preceding scans. On the other hand, multi-way registration optimizes all transforms at the same time, usually by iterating pairwise registrations or by modeling the problem with a single registration objective. MLS correspondences can be used to improve both instances.

Rigid / Non-Rigid Rigid registration methods only allow rigid body transforms for the individual scans, whereas non-rigid methods allow arbitrary ones. However, non-rigid approaches usually regularize the objective in order to avoid degenerate solutions (e.g. by demanding the transform to be as rigid as possible). MLS correspondences can be applied to both types.

Local / Global Local methods use an initial transform estimation (e.g. provided by the user) and refine this transformation to optimize an objective. Global methods do not require any input other than the geometry and find the registration transforms with arbitrary initial alignment of scans. Such global methods usually produce coarse registrations that can be refined with local methods. Since the correspondences used by global methods are not based on spatial proximity (but on, e.g., geometric feature descriptors), MLS correspondences cannot be applied directly.

Correspondence Types Given a set of correspondences, the residuals of the optimization objective can be formulated in various forms. The traditional ICP algorithm (Besl and McKay, 1992) used point-to-point distances, which require a minimum of data and can be defined solely based on point positions. Point-to-plane correspondences (Chen and Medioni, 1991; Low, 2004) that aim at producing transforms that map a point from one scan onto a tangent plane of the other scan were introduced to improve registration performance in flat regions where point-to-point correspondences result in slow convergence. Generalized ICP (Segal et al., 2009) uses additionally plane-to-plane correspondences and considers traditional ICP as special case.

Sampling Discrepancy To overcome the discrepancy in sampling, multiple alternatives have been proposed. Chen and Medioni (Chen and Medioni, 1991) project points from the source shape onto their closest position in the target depth image with an iterative algorithm now known as *normal shooting* (Rusinkiewicz and Levoy, 2001). The resulting point will yield an interpolated closest point on the target. While retaining the theoretical maximum convergence rate provided by closest-point correspondences, this approach depends heavily on the smoothness of the target shape in the neighborhood of the closest point. If the scanning setup is known, the source points can be projected onto the bilinearly interpolated depth map of the target scan (Blais and Levine, 1995; Neugebauer, 1997).

We will refer to these methods as *reverse calibration* (Blais and Levine, 1995; Neugebauer, 1997). The projection is done from the scanner's view point and will generally not be a closest-distance match.

While sacrificing the theoretical convergence guarantees offered by closest-distance correspondences, this scheme is simple and makes no additional assumptions about the smoothness of the target surface in the neighborhood of the projection. Vieira et al. (Vieira et al., 2007) complement the registration approach with an intermediate surface reconstruction and find correspondences between scans and the reconstructed surface. This, however, introduces a significant computational overhead, which MLS correspondences avoid while conceptually still utilizing a reconstructed surface. The Adaptive MLS surface (AMLS) based approach (Huang Y et al., 2011) for ICP registration emphasize on the efficiency of the technique to overcome issues as described earlier. The essential concept of the AMLS method is to reconstruct a smooth and accurate representation of a surface for ICP based registration by adaptively selecting the width of a Gaussian kernel based on the principal curvature of the MLS surface through local integral invariant analysis (Yang et al., 2006). However no broad evaluation is presented by (Huang Y et al., 2011) to express the effectiveness of MLS correspondences to overcome various registration problems. Our analysis focuses on providing extensive experiments on several datasets to demonstrate the impressive feature of MLS correspondences especially stressing upon its performance to handle different scenarios. Additionally we also introduce filtering strategies as described in section 4 to trim the correspondences thereby reducing outliers in matching.

Other projection operators like LSP (Liu et al., 2006),LOP (Lipman et al., 2007), and WLOP (Huang et al., 2009) could also be used for registration. MLS projection is more appropriate for iterative registration for the following reasons: The LSP projection is computationally heavy because a single projection optimizes a functional over the entire point cloud. MLS correspondences only consider points in the neighborhood of a query point. LOP and WLOP try to achieve a uniform distribution of samples, which is counter-productive for correspondence search as the correspondences should naturally have a similar distribution as the query points.

Instead of trying to minimize the distance between corresponding entities, (Mitra et al., 2004; Pottmann et al., 2006) estimate the distance field of the underlying surface with local quadratic approximates and directly optimize the distance of the scan and the target surface. Kubacki et al. (Kubacki et al., 2012) integrated multiple depth images into a model represented by implicit moving least squares (IMLS) on a grid based on signed distance function updates. Similar ideas appeared in (Paragios et al., 2003; El Munim and Farag, 2007). However, any such method inherently suffers from discretization artifacts at reasonable resolutions.

Robustness The pure least-squares problem formulation of early approaches breaks down in the presence of many outliers, producing unusable results. The quality of the alignment is further degraded by noise in the data. To make ICP less sensitive to these defects, variants use robust error metrics (Masuda and Yokoya, 1994; Fitzgibbon, 2003; Papazov and Burschka, 2011; Bouaziz et al., 2013; Altantsetseg et al., 2018),prune outliers (Neugebauer, 1997; He et al., 2017), or establish fuzzy correspondences (Chui and Rangarajan, 2003; Cao et al., 2018).

3 METHODOLOGY

While correspondences between scans are essential for a variety of registration methods (see section 2), we base the following explanations on a pairwise rigid ICP framework with point-to-point correspondences for reasons of notational brevity. However, generalization to other methods is straightforward.

In order to formalize the role of correspondences in the framework of ICP, we first introduce the problem statement for pairwise rigid registration. The aim is to find a rigid body transform $(R,\vec{t})$ composed of rotation R and translation $\vec{t}$ that optimally aligns the source shape $\hat{P}$ to the target shape $\hat{Q}$, each represented by a set of points $P = \{p_i \in \mathbb{R}^3\}$, $Q = \{q_i \in \mathbb{R}^3\}$. Note that both sets generally contain different numbers of points. Using the result $(R_{k-1},\vec{t}_{k-1})$ of a previous step, each iteration updates the transform according to the following optimization objective:

$$\underset{R_k,\vec{t}_k}{\operatorname{argmin}} \sum_{p\in P} d\left(R_k p+\vec{t}_k, \varphi(R_{k-1}p+\vec{t}_{k-1}, Q)\right), \quad (1)$$

where $d : \mathbb{R}^3 \times \mathbb{R}^3 \to \mathbb{R}_+$ is a distance metric between two points, and the function $\varphi(x,Q)$ maps a given point x to its correspondence from the target shape $\hat{Q}$. In classical ICP, φ selects the closest element of the point set Q and the distance metric is the ℓ_2-norm:

$$\varphi_{ICP}(x,Q) = \underset{q\in Q}{\operatorname{argmin}} \|q-x\|_2 \quad (2)$$

$$d_{ICP}(x,q) = \|q-x\|_2^2 \quad (3)$$

This scheme is usually refined by subsampling the source point set P in (1) and by filtering out spurious correspondence outliers. We will elaborate on these filtering techniques in section 4.

4 MLS CORRESPONDENCES

The MLS surface defined from a point set has some interesting properties that make it particularly well-suited for registration purposes. First, the surface is two-manifold, regardless of potential scanning artefacts (Levin, 1998). This allows the correspondences to overcome sampling discrepancy. Second, the surface is smooth and de-noised. As a result, the underlying optimization problem gets better conditioned, which makes it less likely to get stuck in local minima.

In the following section, we explain how to obtain the MLS correspondence for a given query point in a target shape $\hat{Q}$ represented by a point set Q. Similar to a simple nearest-point query, no additional information is required to calculate the correspondence.

We base the correspondence definition on *point set surfaces* (Levin, 2004; Alexa et al., 2001) because their definition makes them particularly appropriate for point queries, which maps well with the correspondence finding problem (see section 3). A projection operator $P_Q(x)$ is constructed that projects query points onto the MLS surface induced by the point set Q. Using this operator, an MLS surface $\mathcal{S}_Q = \left\{x \in \mathbb{R}^3 \mid P_Q(x) = x\right\}$ is defined as the set of points that project onto themselves. The projection procedure consists of two steps:

1. Given a query point p, find an optimal planar reference domain H_{ref} by weighted plane-fitting to the target shape samples $q_i \in Q$. Representing the plane in Hessian normal form with normalized normal $\vec{n}$ and distance D, this corresponds to solving the constrained optimization problem

$$\underset{n,D,\|n\|=1}{\arg\min} \sum_{i=1}^{m} (\langle n,\ q_i\rangle - D)^2\, \theta(\|q_i - \pi_{n,D}(p)\|) \quad (4)$$

   Here, $\pi_{\vec{n},D}(p)$ is the orthogonal projection of p onto the reference domain and $\theta : \mathbb{R} \to \mathbb{R}$ is a weight function. Note that this optimization problem is non-linear as the weights depend on H_{ref}.

2. Approximate the samples q_i locally in H_{ref} by a bivariate polynomial $g(x)$:

$$\underset{g}{\arg\min} \sum_{i=1}^{m} (g(q_{i,H}) - f_i))^2\, \theta(\|q_i - \pi_{\vec{n},D}(p)\|), \quad (5)$$

   where $q_{i,H} \in \mathbb{R}^2$ is the 2D location of q_i in the reference domain H_{ref}, and f_i is the associated height of q_i over the plane.

The projection of the query point p onto the MLS-Surface $\mathcal{S}_Q$ is then defined as $P_Q(p) = \pi_{\vec{n},D}(p) + g(\vec{0})\vec{n}$.

We use the Wendland radial basis function of degree 5 and support radius r as weighting function $\theta(d)$ for its C^2 smoothness (Wendland, 1995):

$$\theta_r(d) = \begin{cases} \frac{(r-d)^4(r+4d)}{r^5} & 0 \le d < r \\ 0 & \text{otherwise} \end{cases} \quad (6)$$

Its compact support makes it possible to efficiently find all contributing points in the target surface by querying a suitable spatial data structure for all points within the radius r. In most of our experiments, we have fine tuned the radius parameter r presented in Table 2 in a way that it is considered as a multiple of the average sampling distance defined in Equation 11.

Iterative projection The MLS projection operator P_Q maps naturally to the correspondence matching function φ_{MLS}:

$$\varphi_{\text{MLS}}(x, Q) \ = \ P_Q(x) \quad (7)$$

To find this projection efficiently, we use an iterative algorithm similar to (Adamson and Alexa, 2003) (see Algorithm 1).

Algorithm 1 Iterative MLS projection

procedure $\varphi_{\text{MLS}}(p, Q)$
  $s \leftarrow p$ ▷ start iteration with query point p
  repeat
    for $q \in Q$ **do** ▷ weight q w.r.t. to current s
      $w_q \leftarrow \theta(\|q - s\|)$
    $\overline{q} \leftarrow$ WeightedMean(Q, w_Q)
    $T = [\vec{u}\ \ \vec{v}\ \ \vec{n}] \leftarrow$WeightedPCA$(Q, w_Q)$
    $\pi_p \leftarrow s - \langle s - \overline{q},\ \vec{n}\rangle \cdot \vec{n}$ ▷ project onto H_{ref}
    $g \models$ WeightedFit$(T^T \cdot (Q - \pi_p), w_Q)$
    $s \leftarrow \pi_p + g(\vec{0}) \cdot \vec{n}$ ▷ update projection
  until convergence
  return s

Correspondence Filtering To make ICP more robust, the determined correspondences are usually filtered to avoid outliers (Rusinkiewicz and Levoy, 2001), e.g., based on a maximum distance threshold. Unless otherwise noted, we used filtering based on normal angle for all tested ICP variants (Pulli, 1999). Hence, a correspondence is rejected if the angle between the corresponding normals is larger than a given threshold.

Higher-order geometric information can be used to make the correspondences even more robust (He et al., 2017). Such information like curvature approximations in the form of surface variation (Pauly et al., 2002) are immediately available as a side-product of

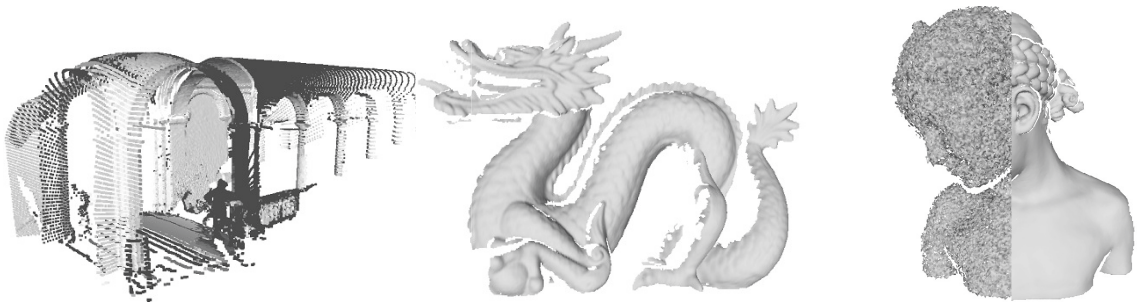

(a) ETH (b) LRF (c) Synthetic (high noise, no noise)

Figure 1: Example point clouds for each of the three datasets we used in our evaluation

MLS correspondences. Given a local principal component analysis in the neighborhood of a reference point with eigenvalues $\lambda_1 \leq \lambda_2 \leq \lambda_3$, mean curvature H can be estimated as (Pauly et al., 2002):

$$H \sim \frac{\lambda_1}{\lambda_1 + \lambda_2 + \lambda_3} \tag{8}$$

For other correspondence schemes, this mean curvature can be pre-computed. We then perform filtering by keeping only correspondences with similar mean curvature. Again, unless otherwise noted, we perform this filtering for all ICP variants.

In summary, we introduce thresholds τ_N on the dot product of normals and τ_H on the mean curvature ratio. We then keep only correspondences that meet the following criteria:

$$\langle \vec{n}_1, \vec{n}_2 \rangle \geq \tau_N \quad \wedge \quad \tau_H \leq \frac{H_1}{H_2} \leq \frac{1}{\tau_H}$$

We found $\tau_N = 0.7$ and $\tau_H = 0.75$ to work well in all our experiments.

Any registration method that can be formulated as MLS-based correspondence matching function can benefit from such correspondences. MLS-correspondences can be made completely transparent and thus be used as a drop-in replacement. No changes to the alignment optimization step are necessary, as long as it computes the residuals over point correspondences. Furthermore, we also support point-to-plane and other types of correspondences by simply adding the necessary data (e.g., the respective surface normal) to the result produced by φ in Equation 3. As compared to (Huang Y et al., 2011), we consider a fine tuned fixed width of Gaussian kernel, however an automatic choice is certainly possible, additionally to reduce the affect of outliers on the correspondences, we introduced a filtering scheme to prune the matches as described earlier in the current section.

5 EVALUATION

To demonstrate the effectiveness of MLS correspondences, we integrated them into SparseICP (Bouaziz et al., 2013) and compared the registration performance of the resulting ICP instance against state-of-the-art fine registration methods. For comparisons, we based our broad analysis on three different datasets with a total of over 40,000 registration problems. Evaluating the methodology on large number of registration pairs with varied difficulty level provides a deep insight on the performance of MLS correspondences integrated into ICP pipeline. We ran all the experiments on an Intel Core i5-6500 clocked at 3.20 GHz. The following section presents how we performed our evaluation. We start by introducing the datasets and the tested methods.

5.1 Datasets

We tested the effect of MLS correspondences on the comprehensive benchmarks provided by (Pomerleau et al., 2013) (which we will refer to as the ETH dataset) and (Petrelli and Di Stefano, 2015) (the LRF dataset).

The ETH dataset comprises six different scenes acquired by an autonomous robot, each containing thousands of registration problems. For each of the registration problems, several initial and the ground truth transform are available.

The LRF dataset contains 23 objects captured by sensors of different quality, ranging from consumer-level depth cameras to professional laser scanners. Out of the 23 objects, we were unable to test four because the implementation of the ReLOC algorithm (Petrelli and Di Stefano, 2015) provided by the authors that is responsible for calculating the coarse initial transforms exceeded the available main memory of our test system (16 GB). The models we did not test are angels, venus, and buste.

Additionally, we synthesized a third dataset from

3D models of publicly available repository. We chose four models (EPFL Statue Model (LGG, 2012), (AIM@SHAPE, 2015) ((Synthetic))) and virtually scanned each from 12 view points uniformly spaced on a circle in the xz-plane centered at the model barycenter. We generated two more variants for each of these scans by adding different amounts of Gaussian noise in the direction of the surface normal (details follow in subsection 5.3, yielding a total of 36 pairwise registration problems per model. Examples of each of these datasets can be found in Figure 1.

5.2 Methods

We compare MLS correspondences with a variety of competing methods. We chose Sparse ICP (Bouaziz et al., 2013) and Generalized ICP (Segal et al., 2009) as representatives of robust ICP variants.

Both of them use closest point matching to find their correspondences. The error metric used during optimization is the point-to-plane metric for the Sparse ICP case and the plane-to-plane metric in the Generalized ICP case (within its probabilistic framework). We will refer to the former as CP-SICP and to the latter as G-ICP.

We augment the Sparse ICP framework with MLS correspondences and denote it by MLS-SICP. Both CP-SICP and MLS-SICP use the normal-based and the curvature-based correspondence filtering strategy detailed in section 4. To allow curvature-based filtering for CP-SICP, we pre-calculated the mean curvatures in a pre-processig step.

As a representative of methods that do not iteratively update correspondences, we chose Fast Global Registration (FGR (Zhou et al., 2016)). Despite its global nature, this methods has been shown to rival the accuracy of local methods. We were unable to test this method on the ETH dataset, since calculating the FPFH features (Rusu et al., 2009) required by FGR proved to be enormously time consuming.

Finally, we include two variants of reverse calibration as outlined in the following.

5.2.1 Reverse Calibration

The first variant is a direct adaptation of (Blais and Levine, 1995; Neugebauer, 1997). The idea is to project a query point onto the bilinearly interpolated depth image from the viewpoint of the scanner. Thus, these variants do not suffer from sampling discrepancy.

To perform the projection, the query point must be brought into the view of the target depth image. We assume that depth images are represented by a map $p : \mathbb{Z}^2 \to \mathbb{R}^3$ of *pixel indices* (u,v) to their associated 3D points (x,y,z). Such a representation is easily obtained if the projection matrix $\mathcal{C}$ of intrinsic parameters of the scanner used to generate the depth image is known. Given a query point p, the corresponding indices into the target depth image can then be computed by performing a perspective projection of the transformed query point onto the target image grid:

$$p' = \mathcal{C} \cdot p \tag{9}$$

After the perspective division, the first and second components of the projected source point yield a real-valued sample location $(u,v) \in \mathbb{R}^2$ with sub-pixel accuracy. This location can be used to bilinearly interpolate the depth value and reconstruct a 3D point using the inverse calibration matrix $\mathcal{C}^{-1}$. We will use this projection as the correspondence for point p and refer to this method as RC-BL (reverse calibration, bilinear).

In cases where more information of the underlying surface is available (in this case, in the form of vertex normals), more elaborate interpolation schemes can be used to produce an interpolation surface that is closer to the actual model surface. We show this option at the example of Phong tessellation (Boubekeur and Alexa, 2008) and denote the resulting strategy as RC-P. Instead of the bilinear interpolation in the depth image, we now perform Phong interpolation, which first calculates the bilinear interpolation at the query location from the depth map. Then, this interpolated point is projected onto the tangent planes defined by the four neighboring depth map samples. Finally, the four projections are bi-linearly interpolated using the original bilinear weights. Since the ETH and the LRF dataset do not provide calibration information, we only performed these experiments on the Synthetic dataset.

5.2.2 Baselines

We derived two additional baselines to examine particular aspects of MLS correspondences. The first baseline aims at isolating the de-noising capabilities of MLS correspondences. Therefore, we project the points of the target scan onto their MLS surface in a pre-processing step, essentially de-noising the target cloud. We then performed Sparse ICP using closest-point matching and the point-to-plane distance. We refer to this baseline as ST-SICP.

The second baseline aims at combining the computational efficiency of Sparse ICP with the accuracy of MLS correspondences in a two-phase process. The first phase performs standard ICP until convergence. Then, the second phase refines the result by performing MLS-SICP. The intuition behind this strategy is to restrict the costlier MLS correspondences to the last

few iterations, where a higher accuracy is needed. We will refer to this baseline as CP-SICP+MLS-SICP. No correspondence filtering is used in the CP-SICP phase so as to avoid any pre-processing that would be required to obtain the normals or eigenvalues of the target cloud points.

5.2.3 Parameters

For all methods other than MLS-SICP, we tried to find the parameter sets that produced the best results, taking into account the parameters suggested by the respective authors. All used parameters can be found in section 8.

5.3 Metrics

After solving the various registration problems with different methods, we evaluate how well the results match the ground truth transforms with a data-dependent metric.

To measure the effect of the registration result on the point clouds, we use the root-mean-square error (RMSE) as our evaluation metric as presented by many other registration papers. Indeed, we strongly believe that RMSE is a good option as it directly measures how well the points are aligned instead of some abstract space. The RMSE measures the error in all point locations for a given transform T_r w.r.t. ground truth T_g:

$$\text{RMSE}(T_r) = \frac{1}{\overline{d}} \sqrt{\frac{1}{n} \sum_{i=1}^{n} \|T_r p_i - T_g p_i\|^2} \qquad (10)$$

The normalization factor $\overline{d}$ represents the sampling distance. For the LRF dataset, where scans are represented as polygon meshes, we use the average mesh length. For the ETH and Synthetic datasets, we use the average distance to the closest neighbor:

$$\overline{d} = \frac{1}{n} \sum_{i=1}^{n} \min_{j \neq i} \|p_i - p_j\| \qquad (11)$$

We use this same unit for setting the standard deviation of the Gaussian noise in the Synthetic dataset, at $\sigma_{\text{low}} = 0.8\overline{d}$ and $\sigma_{\text{high}} = 2\overline{d}$, respectively.

6 RESULTS

In this section, we present the results of our experiments performed on various datasets which verify that MLS correspondences produce more accurate registration results than state-of-the-art approaches. We used various statistical plots to depict our analysis on those datasets. We will also examine various characteristics of the algorithm.

6.1 Accuracy

To compare the accuracy of multiple methods, we performed all registration problems from the datasets introduced in subsection 5.1 and gathered statistics on the final registration RMSE after convergence. The authors of the LRF dataset suggest introducing a threshold of $5\overline{d}$ on the final RMSE to determine whether a registration was successful (Petrelli and Di Stefano, 2015). We adopt this suggestion and only considered results that are below this threshold for all three datasets so as to maintain uniformity among the calculated statistics. The amount of successful registrations for each method on each dataset is presented in Table 1. Every method was considered successful at aligning the view pairs in our Synthetic dataset, despite some results obviously being misaligned (compare Figure 2). This is likely due to our dataset not imposing any additional perturbations beyond the movement of the scanner, and all view pairs being of roughly equal size.

Figure 3 shows the accuracy results for the ETH and LRF datasets. This diagram verifies that the method ML-SICP achieves the lowest RMSE among all tested methods. Additionally, the method also exhibits the least variation in accuracy, indicating that it is more robust than other approaches.

To analyze the accuracy results even closer, Figure 4 shows α-recall plots for the Synthetic dataset. The α-recall of a given RMSE is the percentage of registration problems that achieved an accuracy better than the given RMSE. Hence, the fast-increasing curves represent more accurate registration methods. The MLS-based strategies MLS-SICP and CP-SICP+MLS-SICP are the first curves to rise to the top of the diagram throughout all noise levels. In the no-noise case, this is mostly attributable to overcoming the sampling discrepancy, which most of the other methods suffer from. FGR, which is a strong competitor in these cases, loses accuracy very quickly as more noise is introduced in the data. The Phong interpolation-based reverse calibration variant RC-P, which also overcomes sampling discrepancy, and closest point Sparse ICP CP-SICP work similarly well if no noise is present, despite RC-P not producing closest point matches. All other approaches suffer drastically from noise. Only the MLS-based variants are more resistant as they perform an implicit de-noising of the target point cloud (see Figure 2 for some final alignment examples illustrating this).

6.2 Runtime

We examined the runtime behavior of CP-SICP, the baseline ST-SICP, and MLS-SICP. ST-SICP and

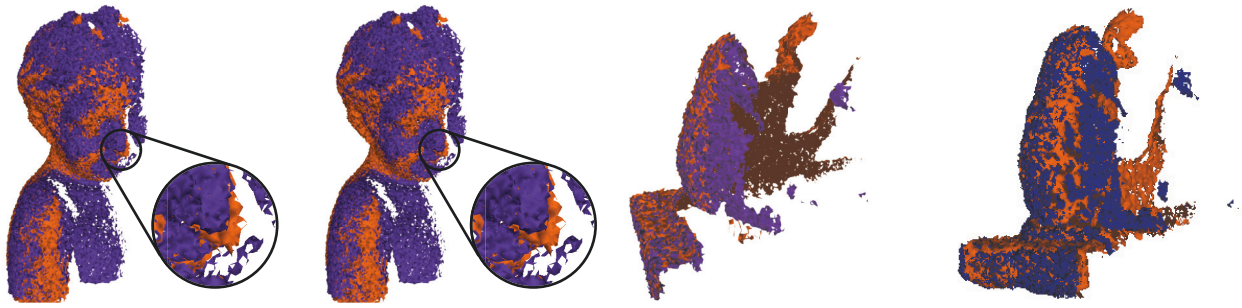

(a) MLS-SICP (RMSE = 0.00081) (b) CP-SICP (RMSE = 0.0303) (c) MLS-SICP (RMSE = 0.00427) (d) CP-SICP (RMSE = 0.012)

Figure 2: Registration results when using MLS correspondences vs. closest point queries for noisy examples from our Synthetic dataset. Note the noticeable deviation from the ideal pose around the nose of the *Bimba* model in case of CP-SICP. In case of the *Monkey* statue, Sparse ICP – using the exact same parameter values except for the correspondence matching strategy – failed to find a valid alignment for this particular view pair (120°against 90°.)

	ETH	LRF	Synthetic
total no. of problems	40,320	4,442	144
RC-BL	–	–	144
RC-P	–	–	144
G-ICP	7460	1530	144
CP-SICP	8567	1459	144
FGR	–	857	144
ST-SICP	10446	1450	144
CP-SICP+MLS-SICP	13847	1793	144
MLS-SICP	14271	1827	144

Table 1: Success rate of pairwise registration on each dataset for each method, as determined by the $5\overline{d}$ threshold proposed by (Petrelli and Di Stefano, 2015).

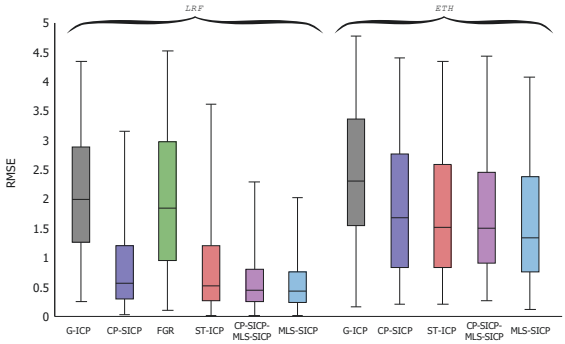

Figure 3: Accuracy comparison of pairwise registration methods for the ETH and LRF datasets. The box height represents the 25th and 75th percentile. The whiskers represent the 5th and 95th percentiles. The middle line represents the median. Better registration results are characterized by lower RMSE values.

MLS-SICP are implemented on top of CP-SICP and thus share the same code base, enabling a meaningful detailed comparison. We performed our analysis on the 12 registration problems from the high-noise version of the *Bimba* model, which represents one moderately difficult example of our Synthetic dataset.

In addition, we measured the time that the 2-step baseline CP-SICP+MLS-SICP took for registering these view pairs and compared it with MLS-SICP. Although we expected that restricting MLS correspondences to the final phase of registration would be faster, CP-SICP+MLS-SICP turned out to be approximately 25% slower on average.

Figure 6 details the runtime composition for registering the first view pair (30°against 0°) from the high-noise *Bimba* set of point clouds. As expected, the computational cost of correspondence matching is greatly increased by the MLS projection. The total time spent on optimizing the rigid transformation, however, has been more than halved in comparison to non-MLS approaches. This is caused by the increased convergence rate (and therefore the reduced number of ICP iterations) that we observed for MLS-SICP. A similar effect – although much more subtle – can be observed for the ST-SICP baseline. However, the reduction in iteration count was insufficient to compensate for the added cost of projecting the target cloud points onto the MLS surface in this case.

Figure 5 shows this effect in more detail, where we plotted the evolution of RMSE over time for different methods. The increased time per iteration and the reduced number of iterations are directly visible by examining the dots in these diagrams. It is also visible that the MLS-based scheme converges to a lower RMSE value, resulting in a higher final accuracy. Although individual registration problems yielded a much higher registration time, most were only slower by a factor of about 2 to 6.

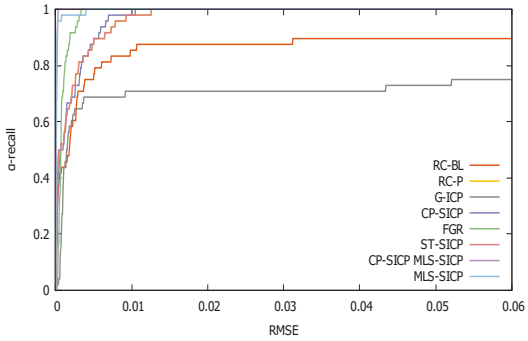

(a) no noise

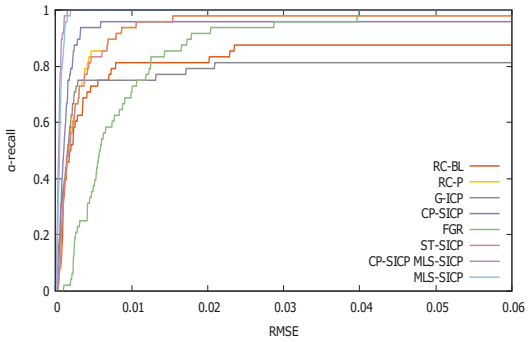

(b) σ_{low}

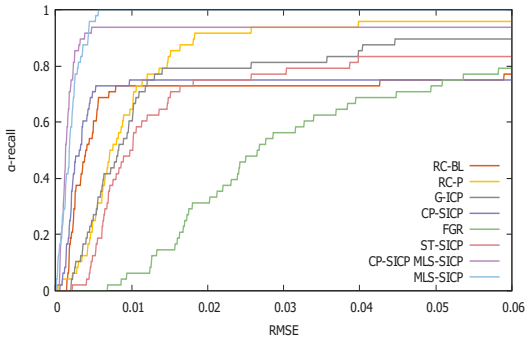

(c) σ_{high}

Figure 4: Accuracy comparison of pairwise registration methods for the Synthetic dataset with different levels of Gaussian noise. The α-recall of RMSE of a method gives a measure of both accuracy and robustness. The slope of the graph represents accuracy, while the maximum recall is a measure of robustness. Steeper and higher is better.

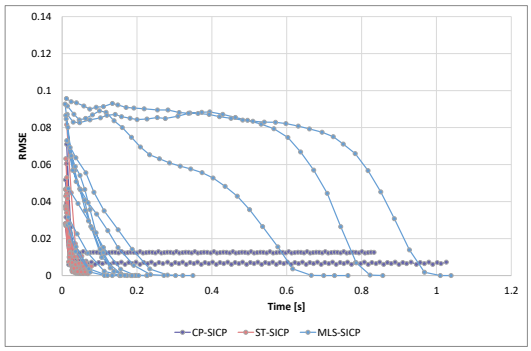

(a) no noise

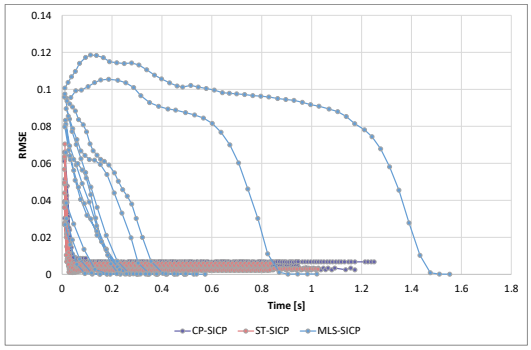

(b) σ_{low}

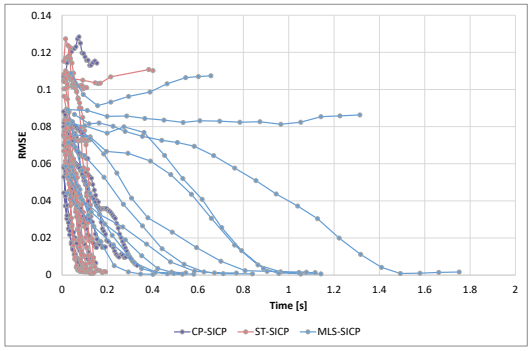

(c) σ_{high}

Figure 5: Convergence behavior of three Sparse ICP variants on the 12 registration problems of the Bimba model. Each curve represents a single registration problem, dots mark the end of an ICP iteration.

6.3 Correspondence filtering

Finally, we examined the effect of filtering mismatched correspondences. Figure 7 shows these results. It is obvious that normal filtering alone is capable of filtering correspondence outliers enough so as to allow a significant increase in final registration accuracy. Additionally performing curvature filtering can improves the accuracy in the range of the upper RMSE quartile even further.

7 CONCLUSION

In this paper, we have presented an analysis of moving least squares correspondences for registra-

	Parameter	Value (ETH dataset)	Value (LRF dataset)	Value (Synthetic dataset)
filtering	τ_N	0.7	0.7	0.7
	τ_H	0.75	0.75	0.75
Sparse ICP	p	0.5	0.5	0.5
	max ICP iters	100	100	100
	max optim. iters (outer)	10	10	10
	max optim. iters (inner)	1	1	1
	distance metric	point-to-plane	point-to-plane	point-to-plane
	sub-sampling	1,000	2,000	2,000
MLS	g	3	3	3
	r	$20\overline{d}$	$20\overline{d}$	σ_0, σ_{low}: $5\overline{d}$ σ_{high}: $8\overline{d}$
	max iters (projection)	20	20	20
Generalized ICP	N	10	10	10
	d_{max}	$20\overline{d}$	$8\overline{d}$	$8\overline{d}$
	ε	0.001	0.1	0.001
Fast Global Reg.	r (FPFH computation)	-	$30\overline{d}$	σ_0, σ_{low}: $10\overline{d}$ σ_{high}: $15\overline{d}$

Table 2: Method parameters used for each method on each dataset. $\overline{d}$ is the average sampling distance (see subsection 5.3).

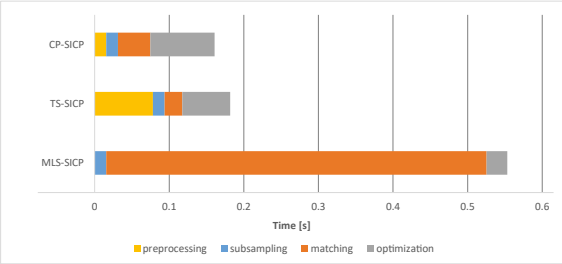

Figure 6: Runtime composition of the three SICP instances for the first registration problem of the Bimba model under high noise. All timings are measured in seconds. The preprocessing step comprises the covariance analasys at each target point for `CP-SICP`, and MLS projection of all target points for `ST-SICP`

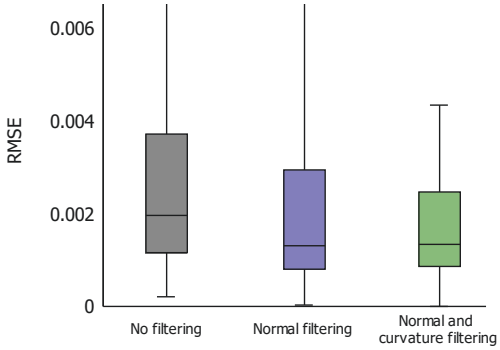

Figure 7: Statistics on final registration RMSE over the Synthetic dataset using different filtering strategies

tion. Due to the implicit surface reconstruction, MLS correspondences allow a significantly higher registration accuracy than state-of-the-art methods. The denoising properties of MLS make registration procedure especially robust to low-quality data.

The MLS-based registration scheme is considerably slower than other approaches. However, we consider the additional runtime a modest overhead for the achieved increase in accuracy. The robustness of the MLS correspondences as compared to nearest neigbor matches could help algorithms achieve better accuracy. The experiments performed as part of the analysis on variety of dataset also points in the same direction. We have also presented a comparison with state-of-the-art ICP based approach along with a global registration method to demonstrate its capability to achieve superior statistical measures clearly expressing its robustness.

We assumed that the amount of noise in the dataset can be estimated, e.g., from the scanner's characteristics. This knowledge allows the definition of a reasonable support radius of the weighting function θ, which is important for achieving a good performance of MLS-based registration. If this knowledge is not available or a wrong estimation is used, the MLS operator may either over-smooth the data and thus result in a loss in accuracy, or it may not be able to de-noise the data enough with negative effects on the convergence rate.

Through an intensive experimentation, we examined the effect of MLS correspondences on diverse dataset in a framework for rigid pairwise registration. Investigating its usefulness in other registration contexts like non-rigid or multi-way registrations is an interesting direction for future research. We believe that the rather separated nature of the correspondence determination step in most registration pipelines helps to make an adaptation of MLS correspondences to other systems straightforward.

REFERENCES

(2012). Statue model repository. http://http://lgg.epfl.ch/statues_dataset.php.

Adamson, A. and Alexa, M. (2003). Approximating and intersecting surfaces from points. In *Proceedings of the 2003 Eurographics/ACM SIGGRAPH Symposium on Geometry Processing*, SGP '03, pages 230–239, Aire-la-Ville, Switzerland, Switzerland. Eurographics Association.

AIM@SHAPE (2015). Digital shape workbench - shape repository.

Alexa, M., Behr, J., Cohen-Or, D., Fleishman, S., Levin, D., and Silva, C. T. (2001). Point set surfaces. In *Proceedings of the Conference on Visualization '01*, VIS '01, pages 21–28. IEEE Computer Society.

Altantsetseg, E., Khorloo, O., and Konno, K. (2018). Rigid registration of noisy point clouds based on higher-dimensional error metrics. *The Visual Computer*, pages 1–10.

Bellekens, B., Spruyt, V., and Maarten Weyn, R. B. (2014). A survey of rigid 3d pointcloud registration algorithms. In *Fourth International Conference on Ambient Computing, Applications, Services and Technologies, Proceedings*, pages 8–13. IARA.

Besl, P. J. and McKay, N. D. (1992). A method for registration of 3-d shapes. *IEEE Transactions on Pattern Analysis and Machine Intelligence*, 14(2):239–256.

Blais, G. and Levine, M. D. (1995). Registering multiview range data to create 3d computer objects. *IEEE Transactions on Pattern Analysis and Machine Intelligence*, 17(8):820–824.

Bouaziz, S., Tagliasacchi, A., and Pauly, M. (2013). Sparse iterative closest point. In *Proceedings of the Eleventh Eurographics/ACMSIGGRAPH Symposium on Geometry Processing*, SGP '13, pages 113–123. Eurographics Association.

Boubekeur, T. and Alexa, M. (2008). Phong tessellation. In *ACM SIGGRAPH Asia 2008 Papers*, SIGGRAPH Asia '08, pages 141:1–141:5, New York, NY, USA. ACM.

Cao, Y.-P., Kobbelt, L., and Hu, S.-M. (2018). Real-time high-accuracy three-dimensional reconstruction with consumer rgb-d cameras. *ACM Transactions on Graphics (TOG)*, 37(5):171.

Chen, Y. and Medioni, G. (1991). Object modeling by registration of multiple range images. In *Proceedings. 1991 IEEE International Conference on Robotics and Automation*, pages 2724–2729 vol.3.

Chui, H. and Rangarajan, A. (2003). A new point matching algorithm for non-rigid registration. *Computer Vision and Image Understanding*, 89(2-3):114–141.

El Munim, H. A. and Farag, A. A. (2007). Shape representation and registration using vector distance functions. In *Computer Vision and Pattern Recognition, 2007. CVPR'07. IEEE Conference on*, pages 1–8. IEEE.

Fitzgibbon, A. W. (2003). Robust registration of 2d and 3d point sets. *Image and Vision Computing*, 21(13):1145 – 1153. British Machine Vision Computing 2001.

He, Y., Liang, B., Yang, J., Li, S., and He, J. (2017). An iterative closest points algorithm for registration of 3d laser scanner point clouds with geometric features. *Sensors*, 17(8):1862.

Huang, H., Li, D., Zhang, H., Ascher, U., and Cohen-Or, D. (2009). Consolidation of unorganized point clouds for surface reconstruction. *ACM transactions on graphics (TOG)*, 28(5):176.

Huang Y, Z. L., Tan Z, W. Q., and L., C. (2011). Adaptive moving least-squares surfaces for multiple point clouds registration. *ASME 2011 International Design Engineering Technical Conferences and Computers and Information in Engineering Conference*, pages 105–113.

Kubacki, D., Bui, H., Babacan, S., and Do, M. (2012). Registration and integration of multiple depth images using signed distance function. In *Computational Imaging X*, volume 8296, page 82960Z.

Levin, D. (1998). The approximation power of moving least-squares. *Math. Comput.*, 67(224):1517–1531.

Levin, D. (2004). Mesh-independent surface interpolation. In Brunnett, G., Hamann, B., Müller, H., and Linsen, L., editors, *Geometric Modeling for Scientific Visualization*, pages 37–49, Berlin, Heidelberg. Springer Berlin Heidelberg.

Lipman, Y., Cohen-Or, D., Levin, D., and Tal-Ezer, H. (2007). Parameterization-free projection for geometry reconstruction. *ACM Transactions on Graphics (TOG)*, 26(3):22.

Liu, Y.-S., Paul, J.-C., Yong, J.-H., Yu, P.-Q., Zhang, H., Sun, J.-G., and Ramani, K. (2006). Automatic least-squares projection of points onto point clouds with applications in reverse engineering. *Computer-Aided Design*, 38(12):1251–1263.

Low, K.-L. (2004). Linear least-squares optimization for point-to-plane icp surface registration. *Chapel Hill, University of North Carolina*, 4(10).

Masuda, T. and Yokoya, N. (1994). A robust method for registration and segmentation of multiple range images. In *Proceedings of 1994 IEEE 2nd CAD-Based Vision Workshop*, pages 106–113.

Mitra, N. J., Gelfand, N., Pottmann, H., and Guibas, L. (2004). Registration of point cloud data from a geometric optimization perspective. In *Proceedings of the 2004 Eurographics/ACM SIGGRAPH symposium on Geometry processing*, pages 22–31. ACM.

Neugebauer, P. J. (1997). Geometrical cloning of 3d objects via simultaneous registration of multiple range images. In *Proceedings of 1997 International Conference on Shape Modeling and Applications*, pages 130–139.

Papazov, C. and Burschka, D. (2011). Stochastic global optimization for robust point set registration. *Computer Vision and Image Understanding*, 115(12):1598–1609.

Paragios, N., Rousson, M., and Ramesh, V. (2003). Non-rigid registration using distance functions. *Computer Vision and Image Understanding*, 89(2-3):142–165.

Pauly, M., Gross, M., and Kobbelt, L. P. (2002). Efficient

simplification of point-sampled surfaces. In *IEEE Visualization, 2002. VIS 2002.*, pages 163–170.

Petrelli, A. and Di Stefano, L. (2015). Pairwise registration by local orientation cues. *Computer Graphics Forum*, 35(6):59–72.

Pomerleau, F., Colas, F., Siegwart, R., and Magnenat, S. (2013). Comparing icp variants on real-world data sets. *Autonomous Robots*, 34(3):133–148.

Pottmann, H., Huang, Q.-X., Yang, Y.-L., and Hu, S.-M. (2006). Geometry and convergence analysis of algorithms for registration of 3d shapes. *International Journal of Computer Vision*, 67(3).

Pulli, K. (1999). Multiview registration for large data sets. In *3-D Digital Imaging and Modeling, 1999. Proceedings. Second International Conference on*, pages 160–168. IEEE.

Rusinkiewicz, S. and Levoy, M. (2001). Efficient variants of the icp algorithm. In *Proceedings Third International Conference on 3-D Digital Imaging and Modeling*, pages 145–152.

Rusu, R. B., Blodow, N., and Beetz, M. (2009). Fast point feature histograms (fpfh) for 3d registration. In *2009 IEEE International Conference on Robotics and Automation*, pages 3212–3217.

Salvi, J., Matabosch, C., Fofi, D., and Forest, J. (2007). A review of recent range image registration methods with accuracy evaluation. *Image and Vision Computing*, 25(5):578 – 596.

Segal, A., Haehnel, D., and Thrun, S. (2009). Generalized-icp. In *Proceedings of Robotics: Science and Systems*.

Tam, G. K. L., Cheng, Z. Q., Lai, Y. K., Langbein, F. C., Liu, Y., Marshall, D., Martin, R. R., Sun, X. F., and Rosin, P. L. (2013). Registration of 3d point clouds and meshes: A survey from rigid to nonrigid. *IEEE Transactions on Visualization and Computer Graphics*, 19(7):1199–1217.

Vieira, T., Peixoto, A., Velho, L., and Lewiner, T. (2007). An iterative framework for registration with reconstruction. In *VMV*, pages 101–108. Citeseer.

Wendland, H. (1995). Piecewise polynomial, positive definite and compactly supported radial functions of minimal degree. *Advances in Computational Mathematics*, 4(1):389–396.

Yang, Y.-L., Lai, Y.-K., Hu, S.-M., and Pottmann, H. (2006). Robust principal curvatures on multiple scales. In *Proceedings of the Fourth Eurographics Symposium on Geometry Processing*, SGP '06, pages 223–226, Aire-la-Ville, Switzerland, Switzerland. Eurographics Association.

Zhou, Q.-Y., Park, J., and Koltun, V. (2016). Fast global registration. In Leibe, B., Matas, J., Sebe, N., and Welling, M., editors, *Computer Vision – ECCV 2016*, pages 766–782. Springer International Publishing.

8 APPENDIX

Please refer to Table 2 for the parameters we used for obtaining the results of the method comparison in section 6.